Simulation of Pollen Transport by Wind: II. Numerical Experiments and Comparisons with Observations

E Novotny [a] and J. Perdang [b]

[a] Scientists for Global Responsibility, Unit 2.8, Halton Mill, Mill Lane, Halton, Lancaster, Lancs., LA2 6ND, United Kingdom
E-mail: evan@sgr.org.uk
[b]Astrophysique Bât. B5, 17, Allée du Six Août, B-4000 Liège, Belgium

Abstract. The Cellular Automaton model described in Paper I has been used to perform simulations of wind-dispersal and deposition of pollen. One set of simulations explores the effects of overall wind velocity, of complex wind components and of size of the field providing the pollen. Plausible values have been assumed for the parameters describing the wind and the production and deposition of pollen, and the results are presented as plots of the amounts of deposited and of air-borne pollen as a function of distance from the source. We find that the geometry of the area covered by the deposit in the down-wind direction may vary from a section of an elongated 'ellipse' to fingers and patchy patterns. Other simulations have been performed using suitable approximations to wind data supplied by the UK Meteorological Office and to published data on pollen creation and release. These simulations are compared with published field observations of pollen deposition and demonstrate that CA modelling provides a good approximation to actual pollen deposition as a function of distance.

Keywords: : simulation, cellular automaton, pollen transport, pollen deposition, gene flow.

1. Introduction

In Paper I, we described the cellular automaton (CA) model and discussed the physical assumptions made in our modelling of pollen creation, release, transport by wind and deposition. We showed how the program can be used to track the progress of wind-driven pollen across a landscape, from its creation to its deposition. In this paper, we first explore the effects of the following inputs to the simulations: various low-level, horizontal wind components (uniform wind, directional variability, turbulence, gusts); and size of the source field. Further numerical experiments compute the percentages of the amount of pollen deposited at various distances from the near edge of the source field and compare the results with observations for various grasses and for maize.

2. CA parameters

The main parameters entering our CA model are summarised in Table 1 and are the same as in Paper I. The actual velocity field, of general components $v_x(x,y,t)$, $v_y(x,y,t)$, will be briefly discussed for each specific experiment. The Table indicates only the uniform (*i.e.,* space-independent) velocity component, w, directed along the x-direction. This component is required to obey the inequality $w \leq 1$ (when expressed in dimensionless form), so that the pollen will be carried no farther than one cell down the lattice in each time-step.

Table 1. Main model parameters. The second column gives the dimensional scaling factor.

The parameters s, Δt and Δa serve as our units of length, of time and of amount of pollen in the CA model. For example, if the wind velocity in a particular cell and at a particular time-step is v (a pure number, say 0.1), then, in a particular application, if Δs is assigned the value 50 m and Δt is assigned the value 10 sec, the wind velocity is $v\,\Delta s/\Delta t$ = 0.5 m/sec in that cell at that time-step.

v	$\Delta s/\Delta t$	total wind-speed
w	$\Delta s/\Delta t$	steady, uniform wind component down the length of the lattice
v	$\Delta s/\Delta t$	critical wind-speed below which no pollen can be carried off
f_v	1	entrainment factor (fraction of local wind-speed with which pollen is carried}
T	Δt	total duration of a run
T	Δt	total time interval over which all pollen is released (single or multiple spasmodic event)
N	$\Delta a\,\Delta s$	total amount of pollen creatable per unit area
P	Δt	probability of release of pollen per unit area and per unit time-step
P	Δt	probability of deposition and sticking of pollen per unit area of region external to source field and per unit time-step
P	Δt	probability of deposition and sticking of pollen per unit area of source (donor field) and per unit time-step

For each experiment, the numerical values of these parameters will be listed in dimensionless form. For instance we may have

$$w = 0.8;\quad v_c = 0.2;\quad f_v = 0.2;\quad T_{exp} = 300;\quad T_P = 200;\quad N = 5;$$
$$P_c = 1/200;\quad P_{sF} = 0.1;\quad P_{sE} = 0.04.$$

Each numerical experiment represents a 3-parameter family of potential observational situations. In any experiment, the values of P_{sF} and P_{sE} must also be specified, and their dependence on the cell-size and time-step should be noted. In order to describe a specific observational configuration we have to assign actual physical magnitudes to the CA units. For instance, if we choose

$$\Delta s = 50 \text{ m}, \quad \Delta t = 10 \text{ s}, \quad \Delta a = 10^{10} \text{ grains (in a cell)},$$

then we obtain the physical, dimensional model parameters by multiplying the dimensionless list of values by the dimensional factors given in the second column of Table 1. The steady, uniform wind-speed represented in the theoretical model is $w\Delta s/\Delta t = 4$ m s^{-1}. Pollen is carried with a speed of f_v times the wind-speed, or 0.8 m s^{-1} if the non-stationary velocity contributions are negligible. The represented duration of the run is $T_{exp}\Delta t = 3{,}000$ s or 50 min. The number of grains of pollen available per unit area is $N\Delta a/(\Delta s)^2 = 2 \times 10^7$ grains m^{-2}; *etc*. The square donor field has length of side = (20 cells)$\times\Delta s$ = 1 km.

If we had made another choice of the CA units, for instance,

$$\Delta s = 21 \text{ m}, \quad \Delta t = 7 \text{ s}, \quad \Delta a = 3 \times 10^{10} \text{ grains (in a cell)},$$

then the *same numerical experiment* would describe a different field observation, in which we would have a steady, uniform wind-speed of 2.4 ms^1 and a pollen speed of 0.48 m s^{-1} (under the conditions stated). The represented duration of the run would be 2,100 s or 35 min; and the number of grains of pollen per unit area would be 3.4×10^8 grains m^{-2}; *etc*. The length of the donor field would now be 420 m.

In the following series of experiments we investigate the influences of the various parameters and of the nature of the wind profile.

3. Model experiments on effects of wind

3.1 Experiments on effects of entrainment factor f_v and sticking probability P_{sE} in the external field

We performed experiments on deposition for fixed $P_{sF} = 0.1$ and variable P_{sE} and f_v. The effects of the sticking probabilities and of the entrainment factor f_v are inter-dependent: the larger the sticking probability, the smaller the distance that pollen can travel; and the larger the entrainment factor, the farther the pollen can travel.

Fig. 1 shows contour plots of the spatial distributions of air-borne pollen and of deposited pollen at time-step $t = 350$ (about 6 hours after the initial release of pollen), for a set of experiments in which the effects of the parameters P_{sE} and f_v are tested, all other factors being held constant. To the principal, uniform wind component (down the length of the lattice) are added space- and time-dependent components. The sticking probability in the donor field is taken equal to $P_{sF} = 0.1$ (see section 5.2). The source field corresponds to the white square towards the left of the pictures that show the deposits. The essentially exponential colour code exhibits the relative amounts of pollen (in

units of Δa): white (outside the source field) 0; black 1; blue 2; cyan 3-4; yellow 5-8; red 9-16; green 17-32; and again white >32 units (there is no confusion with white 0, since the highest concentrations of pollen occur in the field only).

This figure illustrates in particular (in case c) that high entrainment (factor $f_v = 0.9$) combined with a low sticking probability in the outer region ($P_{sE} = 0.01$) produces a deposit that may extend over the whole lattice space (150 cells, *i.e.*, several kilometres). This pattern occurs at medium strength winds (5-10 m/s). If we increase the outer sticking probability ($P_{sE} = 0.05$) and decrease the entrainment factor ($f_v = 0.40$), the extent of the deposit is naturally reduced (case a). Note that the typical pattern of the amount of airborne pollen at a given time-step is not spatially uniform; it may exhibit high-concentration 'tongues' or 'fingers' parallel to the main wind component. These 'tongues' extend far beyond the average concentration level outside the donor field. A similar observation holds for the pattern of the deposit. In our experiments this result is the consequence of a space-dependent component and a turbulent (time-dependent) component in the wind. A similar effect is brought about by space-dependent sticking probabilities. All other factors being kept constant, the extent of the deposit scales with the average propagation speed of pollen (*i.e.*, with the average wind-speed, and with the factor f_V), as follows from an elementary dimensional argument. We recall that in the real environment, dry weather produces lower sticking probabilities, while wet weather corresponds to higher sticking probabilities.

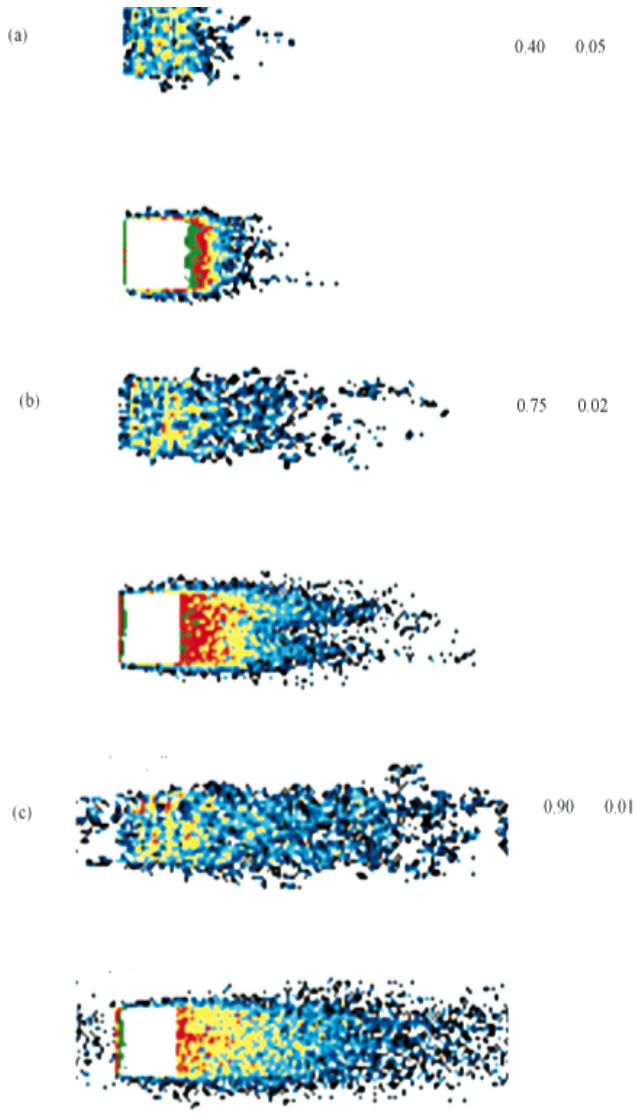

Fig. 1. Contour plots of pollen density for increasing. entrainment factor f_v and decreasing sticking probability P_{sE} at fixed $P_{sF} = 0.1$. In each pair of boxes, the upper box shows airborne pollen and the lower box shows deposited pollen. A boundary condition causes pollen blown out of the lattice to re-enter it at the opposite boundary, as is evident in the last case. The values of f_v and P_{sE} are, respectively: (a), 0.40 and 0.05; (b), 0.75 and 0.02; (c), 0.90 and 0.01. Note that this colour coding (see text) differs from that of Figs. 2-6.

3.2 Experiments on effects of wind conditions and size of source field

We have investigated the possible patterns of pollen deposit that our models can generate when different wind conditions are chosen. For this series, all parameters not referring to the wind are chosen as follows

$$v_c = 0.2; \quad f_v = 0.2; \quad T_{exp} = 900; \quad T_P = 800; \quad N = 50; \quad P_{sF} = 0.01; \quad P_{sE} = 0.005.$$

The parameter P_c is fixed by the integral condition that the total number of pollen grains available in a cell is $N\Delta a \int dt\, P_c(t)$. The lattice is our standard universe of 150×50 cells. The donor field is a square of 20×20 cells or, when doubled, a rectangle of 40×20 cells.

Colours in the figures described below have the following meanings, in units of Δa: white = 0, black = 1, blue = 2-3, cyan = 4-7, yellow = 8-15, red = 16-31, green = 32-63, white (again) = 64. (Note that this colour coding differs from that of Fig. 1.)

On some of the figures, pollen has been blown out of the bounds of the lattice. We have adopted periodic boundary conditions, which force the pollen to re-enter at the side opposite to that at which it left. This computational artefact may be interpreted as pollen blowing in from an identical lattice juxtaposed with the present one on the side through which the pollen enters.

Pollen that remains air-borne at the end of the experiment is plotted separately and is shown above the plot of deposited pollen, in each of the figures. If the experiments had proceeded for a long enough time this pollen would also have been deposited.

In Fig. 2, the wind is uniform in time and space. When the field size is increased, the amount of pollen produced and carried by the wind is also increased. The corresponding increase in deposited pollen is not easily discernible in a comparison of (a) and (b) because only *relative* amounts of pollen are shown, rather than absolute amounts. In (c), as the wind-speed is increased, pollen is deposited farther down the lattice, as expected from dimensional analysis. The long 'fingers' of high pollen density intruding into regions of low pollen density should be noted. This is of particular importance for considerations of separation distances required between compatible crops when genetic segregation is required.

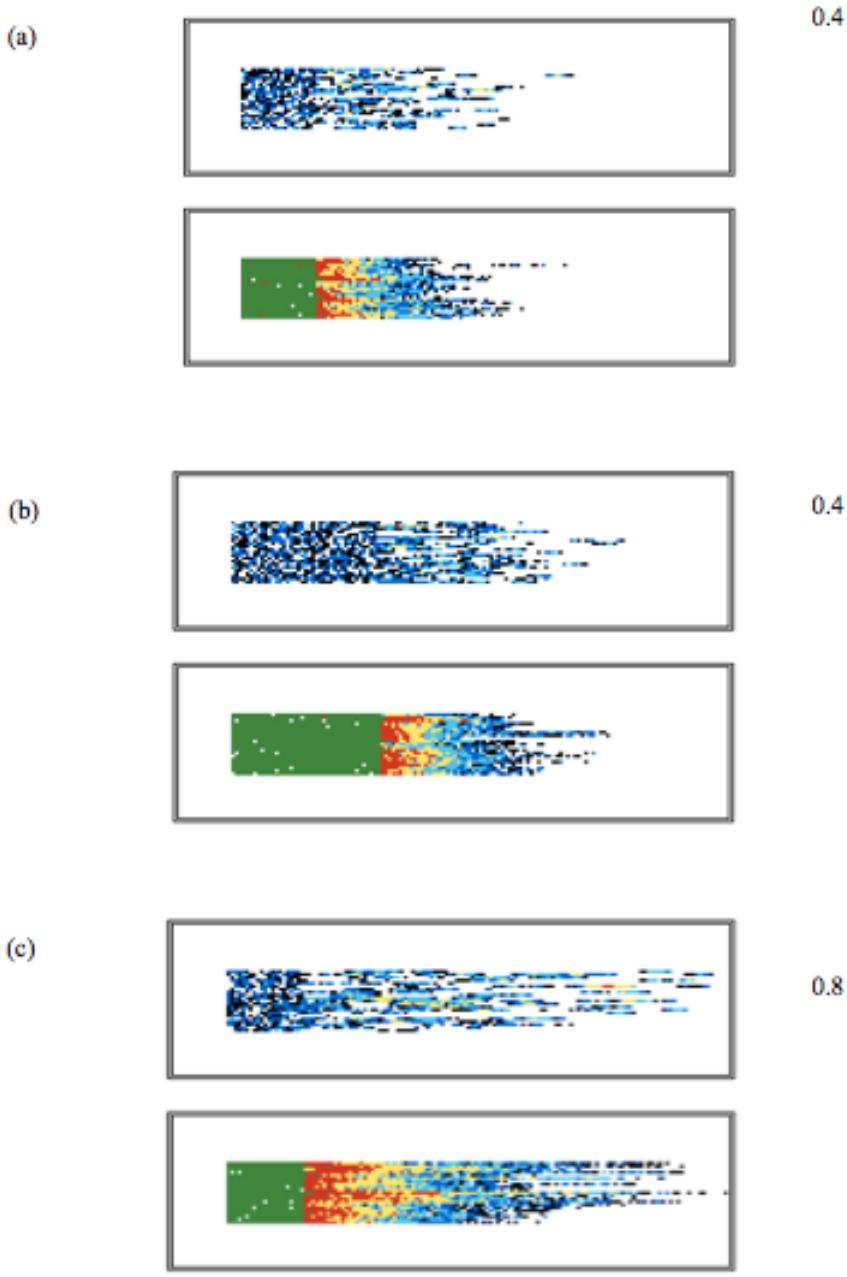

Fig. 2. Uniform, steady, longitudinal wind.

In each of the three pairs of boxes, the upper box shows airborne pollen and the lower box shows deposited pollen.
(a) A wind that is steady and uniform over the lattice blows down the length of the lattice. The wind-speed is $w = 0.4$.
(b) The size of the field has been doubled, but the wind-speed is the same as in (*a*).
(c) The size of the field is again the standard size, as in (*a*), but the wind-speed has been doubled to $w = 0.8$.

Fig. 3 shows the effects of successive increases in a wind that is uniform over space and has a steady, transverse component superimposed on a uniform, steady longitudinal wind of speed $w = 0.8$ in all three cases. The side-wind has speed 0.2 (in frame (a)), 0.4 (in frame (b)) and 0.8 (in frame (c)). In the last case, especially, the pollen becomes widely dispersed. Long 'fingers' are again visible in case (a) and, to a lesser degree, in case (b). In all three cases, the main contours of density are roughly oval.

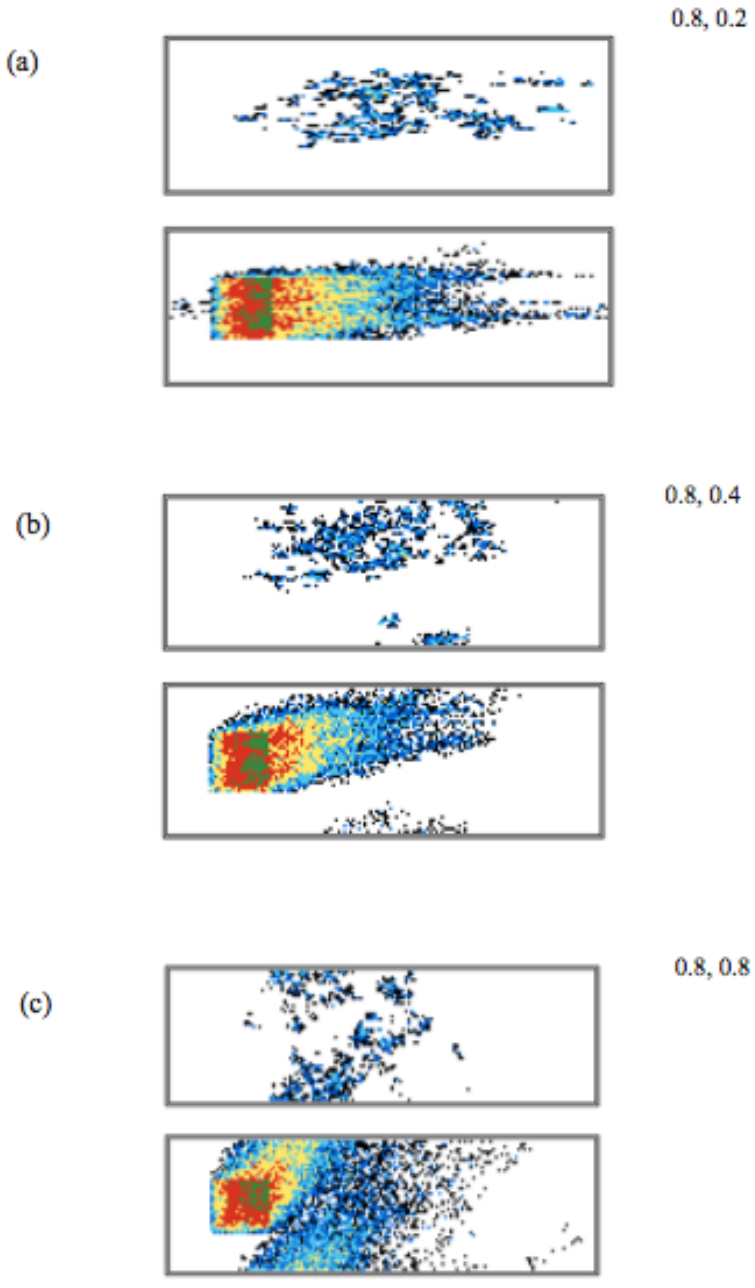

Fig. 3. Uniform, steady, transverse wind component

In each of the three pairs of boxes, the upper box shows airborne pollen and the lower box shows deposited pollen. Pollen blown out of a boundary is shown as re-appearing at the opposite boundary. In all three cases, there is also a uniform, steady longitudinal wind with speed $w = 0.8$.

(a) side-wind-speed = 0.2, (b) side-wind-speed = 0.4, (c) side-wind-speed = 0.8.

Fig. 4 illustrates the effects of a wind that is uniform over space but has a transverse component that is variable in time. Once again, we see long 'fingers, especially in case (*a*), and oval contours in the main deposit.

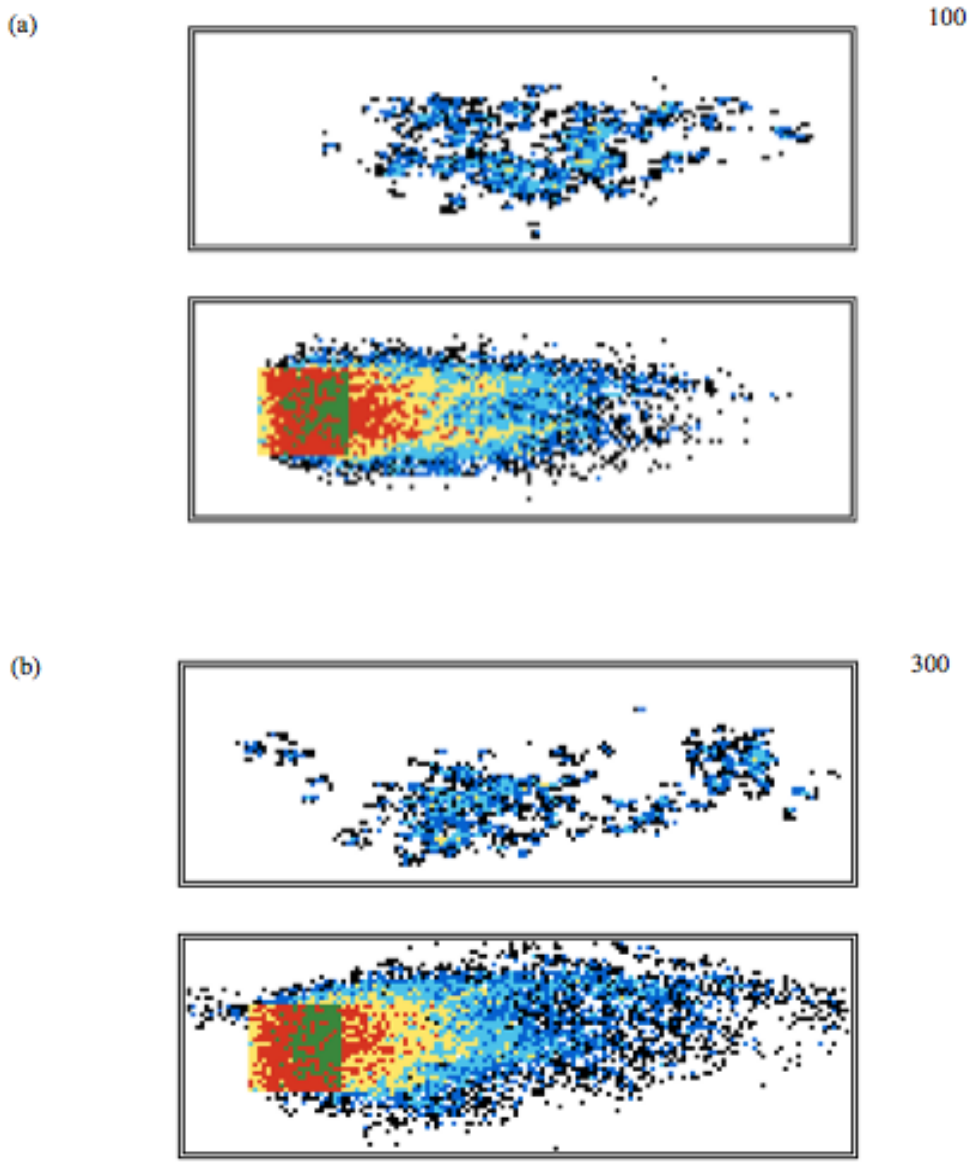

Fig. 4. Uniform, variable, transverse wind component

In each of the three pairs of boxes, the upper box shows airborne pollen and the lower box shows deposited pollen. Pollen blown out of a boundary is shown as re-appearing at the opposite boundary.

Fig. 5 incorporates changes in the side-wind (*i.e.*, transverse wind) that are random in both place and time. As expected, the stronger the side-wind, the greater is the transverse dispersal of the pollen. Essentially, this random transverse effect produces a transverse diffusion. 'Fingers' are visible in cases (a) and (b), while oval contours appear in cases (b) and (c).

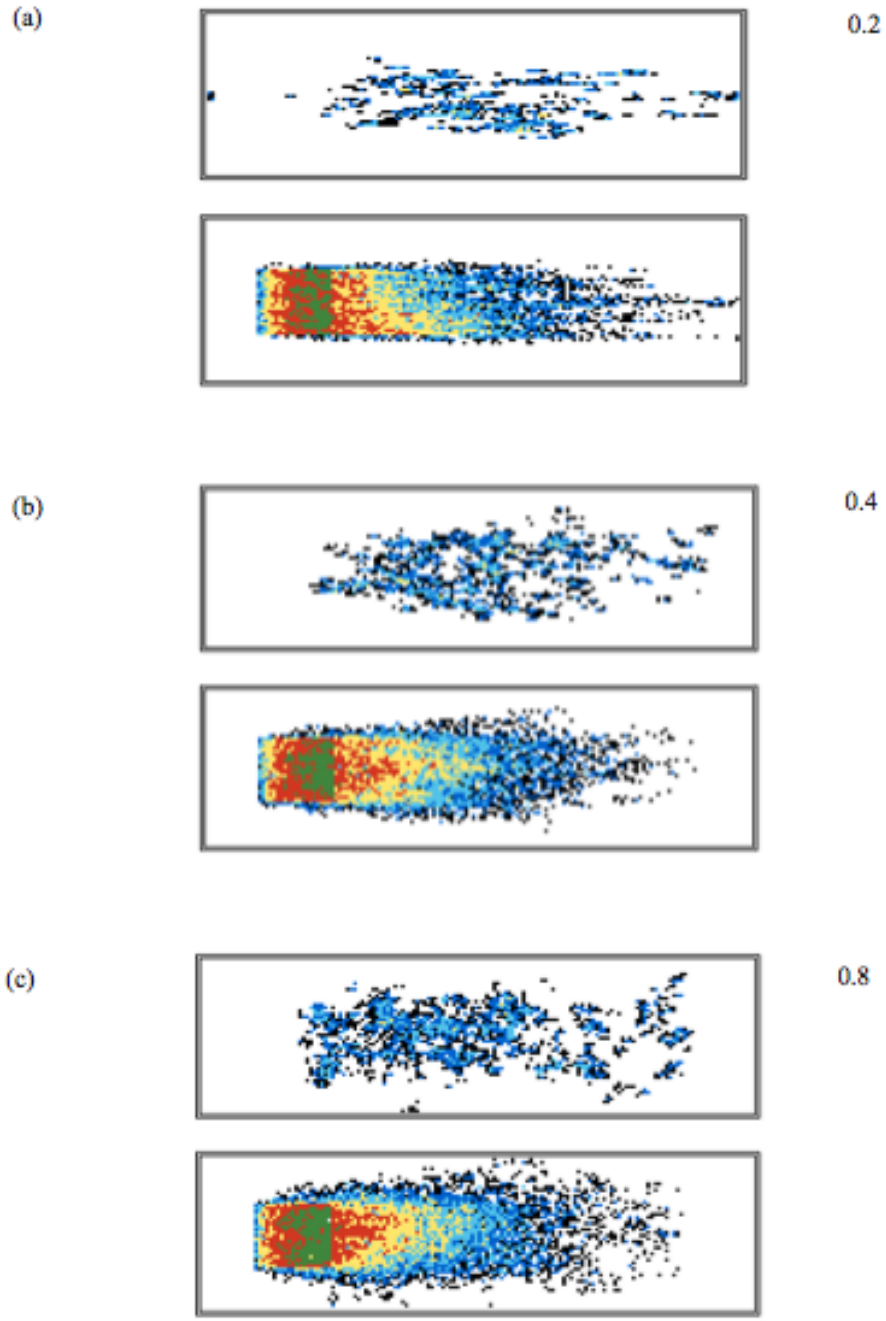

Fig. 5. Non-uniform, variable, transverse wind component.

In each of the three pairs of boxes, the upper box shows airborne pollen and the lower box shows deposited pollen. Pollen blown out of a boundary is shown as re-appearing at the opposite boundary.
(a) There is a steady, uniform longitudinal wind of speed $w = 0.8$; but the side-wind varies randomly at each time-step and at each cell of the lattice. It may assume any of the values $+A$, 0, $-A$, *i.e.*, up, zero, down. The value of A in this case is 0.2. Cases (b) and (c) are similar to (a) but with $A = 0.4$ and 0.8 respectively.

Fig. 6 illustrates the effects of gusting winds. Frame (a) shows a comparison case which takes account of pollen transport by an irregular wind, involving the following components: (1) a component independent of space and time; (2) a wavelike, propagating component of zero average over space and time, which is here given by a complicated expression represented by a Fourier series; and (3) a randomly fluctuating component of zero average. No gusty component is included. In frame (b), in addition to the irregular wind of (a), a gust blows obliquely across the lattice. The peak of the gust occurs at time-step $t = 200$, with diminishing effectiveness at times before and after $t = 200$. The two components of the gust are modelled by the expressions

$$g_x = A \exp\{ - [(t - T_{gust})/50]^2\} \exp\{- [(y + 0.3x - 0.33t)/20]^2\} ,$$
$$g_y = B \exp\{ - [(t - T_{gust})/50]^2\} \exp\{- [(x + 0.3y - 0.23t)/35]^2\} , \qquad (1)$$

with

$$A = 2, B = 4 \text{ and } T_{gust} = 200 .$$

These gusts disperse the pollen more widely in the transverse direction than do the irregular winds (a). The first exponential term in either gust component (Eq. 1) produces a peak at time $t = T_{gust}$, of width of the order of 100 time-steps. The second exponential of each component governs the position of the peak, causing it to travel as time progresses. The maximum effect occurs at positions (x_{gust},y_{gust}) such that the arguments in the second exponentials of Eq. 1 vanish.[1]

Both cases exhibit long streamers of denser pollen, while case (a) shows the typical oval contours in the main pollen deposit.

[1] The effect of the gust is particularly dramatic when the result of the simulation is animated. Initially one observes a deposit gently growing in the direction of the down-wind. A powerful oblique gust then sets in which produces a transverse deposit. After a while, the growth of the deposit becomes regular again.

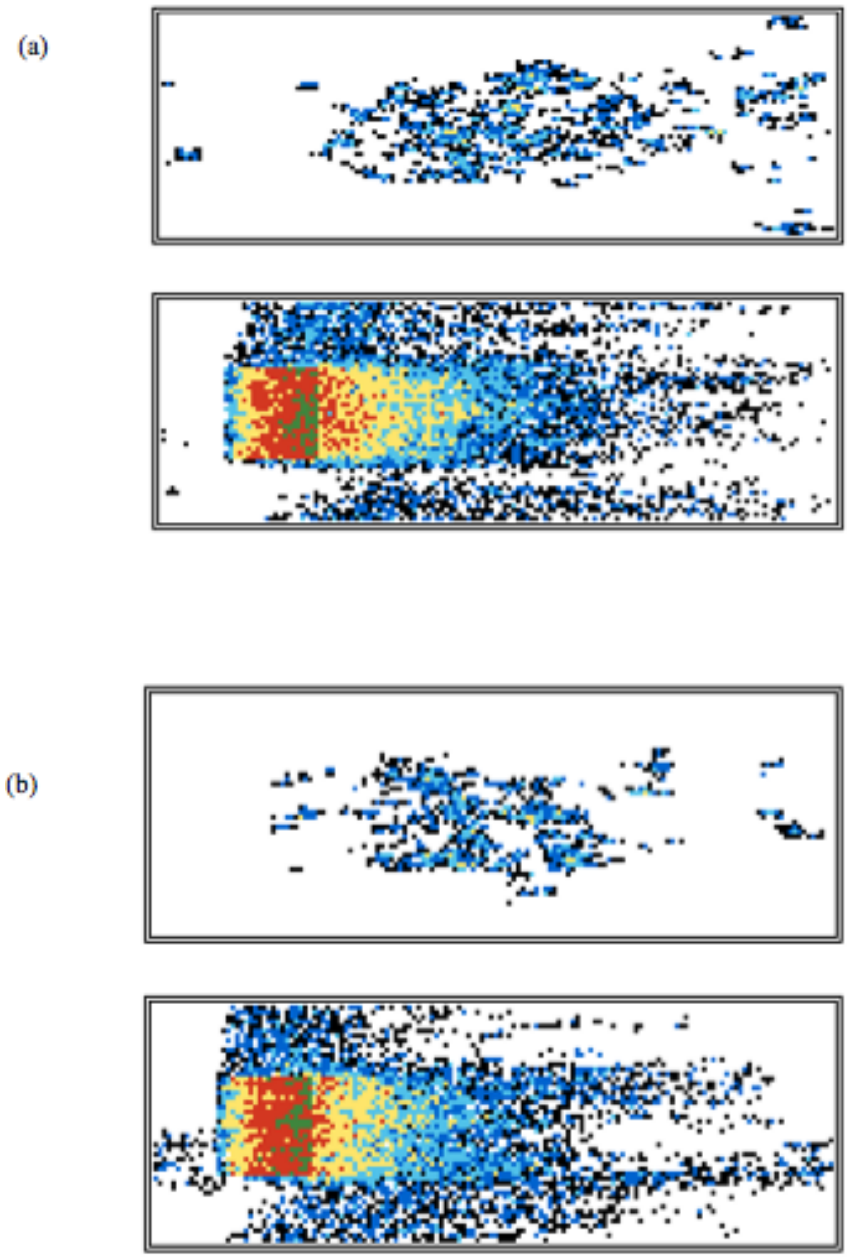

Fig. 6. Irregular wind and gusting wind.

In each pair of boxes, the upper box shows airborne pollen and the lower box shows deposited pollen. Pollen blown out of a boundary is shown as re-appearing at the opposite boundary.
(a) Irregular wind; (b) Irregular wind as in (a) and a superposed gusting wind, as described in the text.

4. Observational data on wind patterns and pollen release

We shall describe numerical experiments designed to be compared with actual observations in the field. To this end, we have obtained observations of wind velocities and of pollen production and release, which we have represented by analytical expressions. Unfortunately, data for the winds that actually prevailed during the field experiments in Oklahoma, USA, with which we shall compare our

CA results, are not available; therefore we have substituted realistic wind data for another location (Dunkeswell, Devon, United Kingdom).

4.1 Wind data

Tables of measured wind-speed and direction were obtained from the UK Meteorological Office. We have data from Dunkeswell aerodrome (in Devon) during July 1995, which best seemed to fit our requirements of a location in a farming region and away from urban areas. An aerodrome, of course, is not an ideal choice; but the data needed for these simulations are relatively scarce. Wind-speeds and directions were measured at an altitude of 10 m. The Dunkeswell data are plotted in Figs. 7 and 8. Also shown are analytical approximations, consisting of summations of sine and cosine terms, which are more convenient to use in a program than the tabulations. Detailed point-by-point agreement between the observed data and the analytical representations is not required, only an overall similarity.

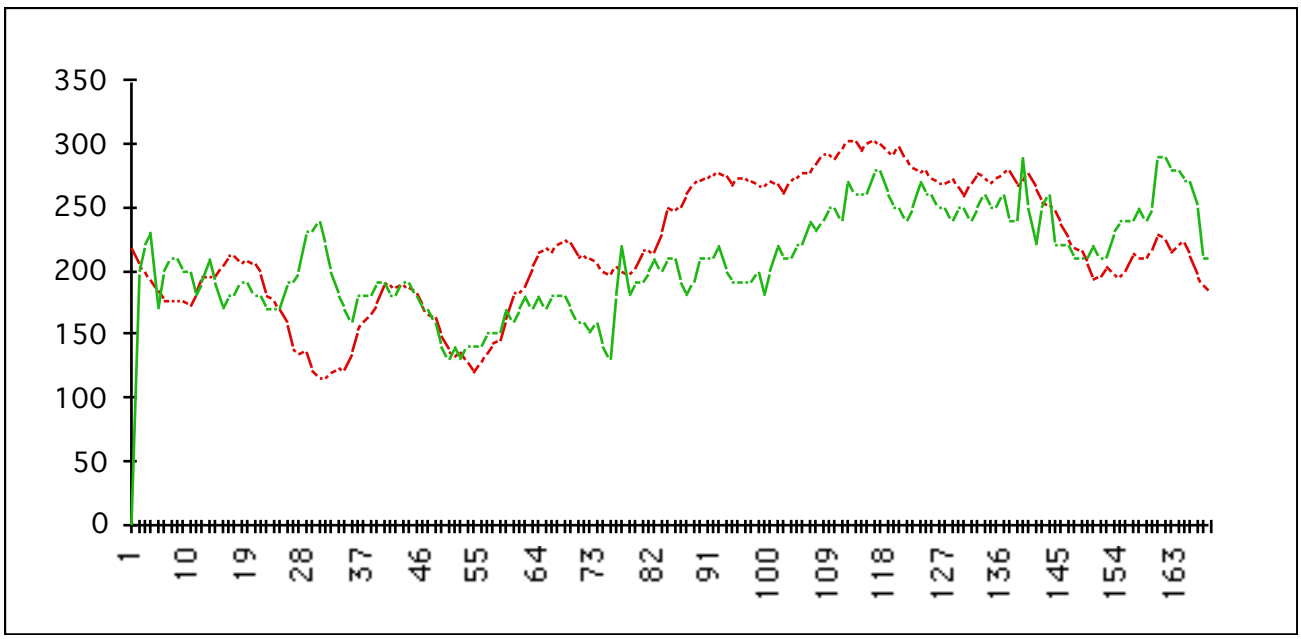

Fig. 7. Dunkeswell wind-direction data (in degrees, green line) and analytic approximation (red line) for a period of 169 hours starting on 11 July 1995 at midnight. (Data from UK Meteorological Office)

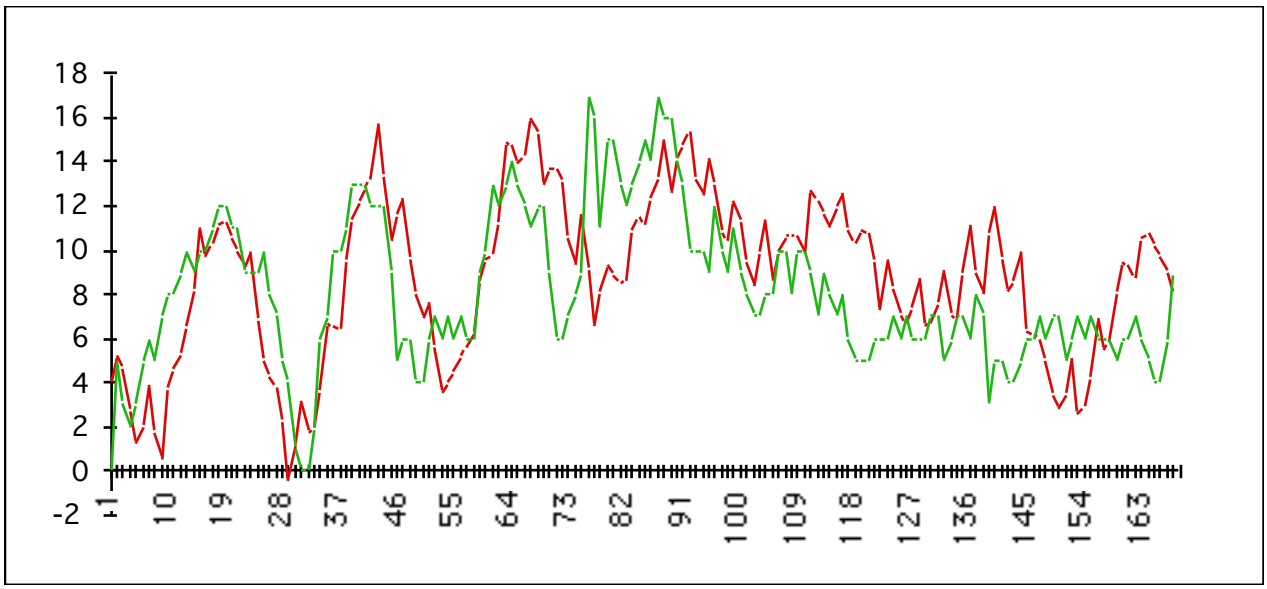

Fig. 8. Dunkeswell wind-speed data (in knots) (green line) and analytic approximation (red line) for a period of 169 hours starting on 11 July 1995 at midnight. In the simulations, wind-speeds above 13 knots have been levelled off. (Data from UK Meteorological Office)

The crops we are considering in our simulations, such as maize, might reach only 2 m, where wind velocity would be smaller than at a height of 10 m. Wind-speed must decrease towards the ground, and a (rather arbitrary) factor 0.7 has been applied to the data to help compensate for the discrepancy in heights. Also, because the wind is allowed to carry pollen no farther than one cell longitudinally in each time-step, the time-step may need to be as low as 2 seconds. At that rate, over 40,000 time-steps would be required to cover a single day. To save a considerable amount of computing time, any peaks of wind-speed rising above 13 knots have been levelled off.

4.2 Pollen data

Release of pollen (or 'creation' of pollen in our applications) does not proceed at a constant rate. Jones and Newell (1946) measured the rates for several grasses and found that pollen release starts early in the morning, builds up until midday to display one or two peaks, and then declines to zero in the evening. During night-time there is no release of pollen. With the small time-steps used in our modelling, proceeding over nights would greatly increase computing time while contributing nothing to pollen deposition. To minimise computing time we have, in fact, taken pollen to be released with a single peak, starting from zero and returning to zero, over the entire duration. The equation used was

$$P_c \propto (t/T_c)(1 - t/T_c) \quad \text{for } 0 \le t \le T_c, \quad \text{and} \quad P_c = 0 \text{ for } t > T_c,$$

where T_c is time at end of creation of pollen.

5. Comparison of model experiments with observations

The experiments we describe in this section are formally carried out with the simple version of the three-dimensional model. The high-altitude wind is, however, set equal to zero, and so are the exchange probabilities between the second and third layers. The relevant parameters (wind pattern, exchange probabilities, *etc.*) are not known well enough to warrant a meaningful theoretical treatment of the high-altitude pollen transport. The actual experiments are therefore two-dimensional. They involve a minimal number of adjustable parameters.

5.1 The parameters

In the following numerical experiment, we keep the geometry of the donor field fixed. This field is modelled by a square area of 20×20 cells, on a lattice of 150×50 cells.

It must be emphasised that the various parameters are not all independent. Changing cell-size implies a corresponding change in wind-speed, while cell-size and wind-velocity together determine the maximum time-step. The creation and sticking probabilities are also necessarily re-valued if either cell-size or time-step is changed (Table 1); and a change in wind-speed requires a change in either cell-size or time-step, hence also in these probabilities.

5.2 Calibration of the sticking probability P_s

An empirical determination of the numerical value of the sticking probability appropriate to a given field situation would be difficult. We resort to a calibration process to find the value that produces the best fit of results from our models to the results from a set of observations of the relative amounts of pollen deposition as a function of distance. Although the sticking probabilities are uniform over a field in our experiments, the program allows this probability to be prescribed for each lattice cell individually.

Fig. 9 shows in colour the measurements of Jones and Newell (1946, p. 38), who performed field experiments to determine, for seven species of grasses, the amounts of pollen deposited on coated glass slides at various distances from the centre of a square source field. Measurements were taken at several heights above ground and along eight equally-spaced radii covering 360 degrees around the source. We have attempted to simulate their observations along one direction with our CA programme. For ease of comparison with CA simulations, the Figure expresses distance in units of our cell-size, which is in the present case 8 m.

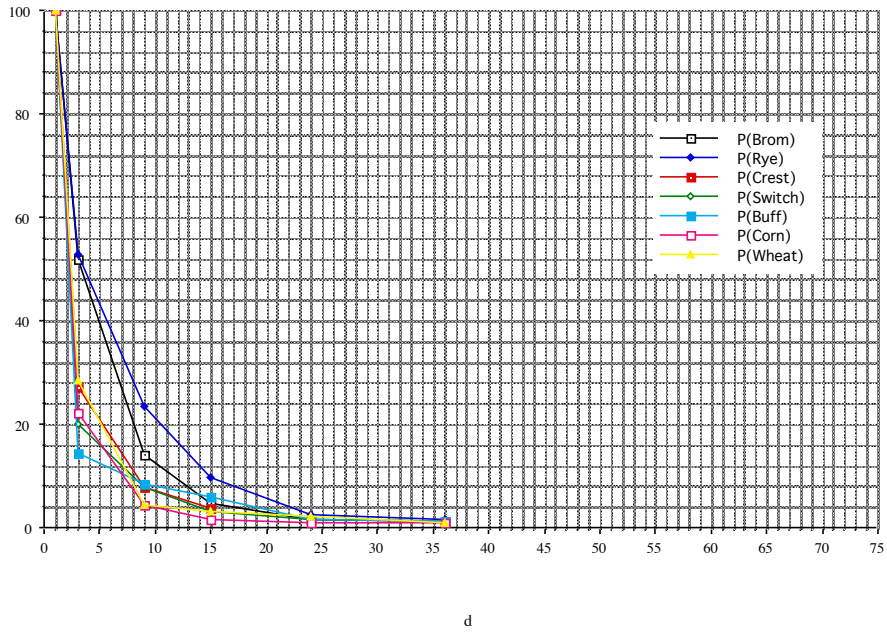

Fig. 9. Percentage of amount of deposited pollen as a function of distance from source, for 7 species of grasses (distance d in numbers of CA cells; 1 cell = 8 m). Data from Jones and Newell (1946).

These observational results will be compared with our CA models for various values of sticking probability $P_{S,}$ shown in Fig. 10.

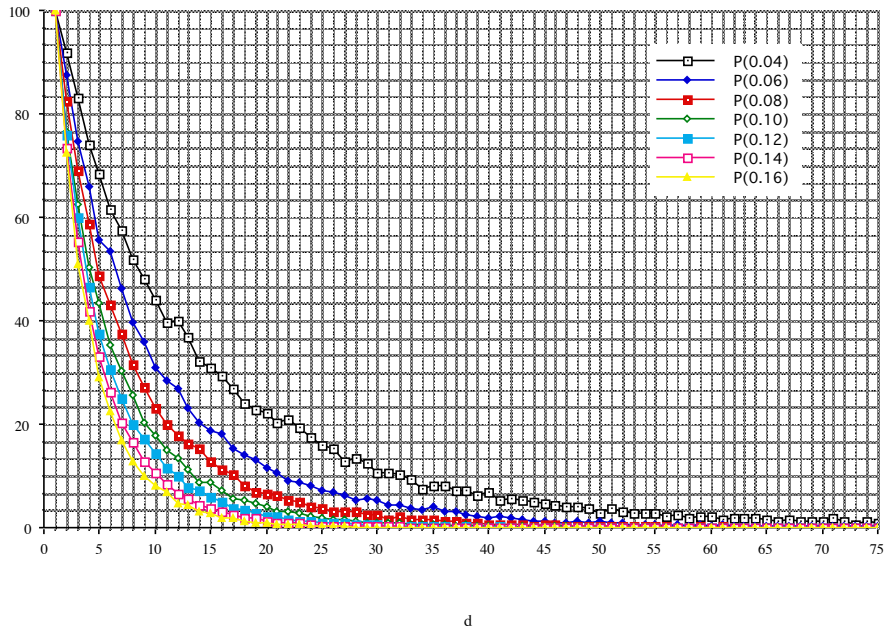

Fig. 10. CA results for percentage of amount of deposited pollen as a function of distance from source, computed for deposition probabilities $P_{sF} = P_{sE}$ (from right to left) 0.04, 0.06, 0.08, 0.10, 0.12, 0.14 and 0.16 (distance d in numbers of CA cells; 1 cell = 8 m).

In Fig. 11, we have superimposed Figs. 9 and 10. An overlap occurs between the upper observational curves and the lower CA model curves. The observational curve for bromegrass (black curve, with open squares, marked 'Brom') fits well the CA curve with P = 0.14 (pink curve, with open squares), while the observational curve for rye (dark blue, with diamonds) lies near the CA curve with P = 0.10 (green curve, with diamonds). We conclude that a reasonable value for P_{sF} is 0.1, which we shall take as a guideline for the experiments described below.

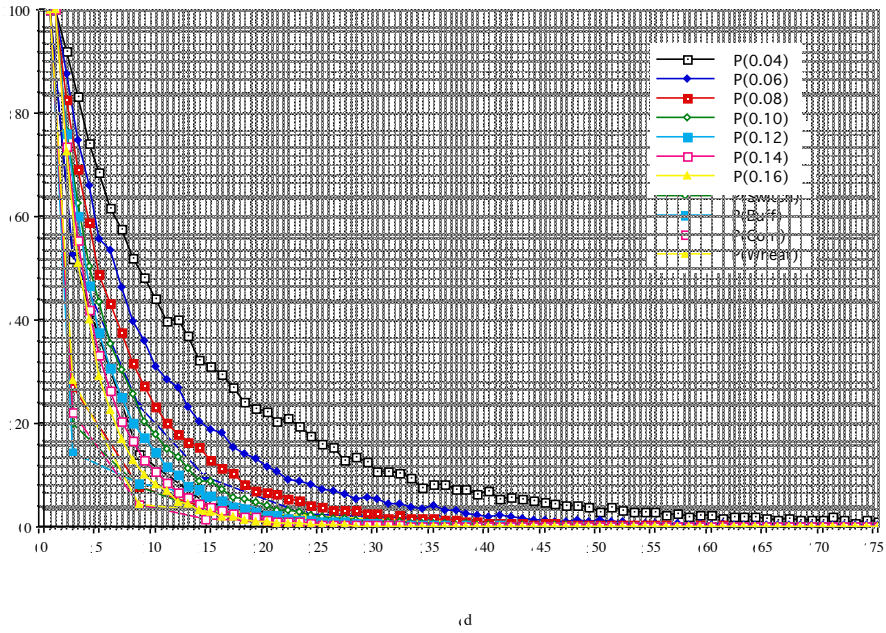

Fig. 11. Superimposition of Figs. 9 and 10. The apparent doubling of some horizontal grid lines arises from the fact that different intervals were used in the two Figures between the primary grid lines for the vertical scale. (Distance d in numbers of CA cells; 1 cell = 8 m).

5.3 Field observations of decline of outcrossing with distance

Jones and Brooks (1950) made field observations in Oklahoma in 1947, 1948 and 1949, measuring the percentages of outcrossing at various distances from a rectangular field of yellow maize. The receptors were maize of a white variety planted in eight blocks of size 10 feet square to the windward side of the donor field, in a pattern staggered to minimise 'shadowing' of one block by another. Outside the blocks was vegetation remaining after "small grains" growing there had been harvested before maize pollination occurred. Distances were measured from the edge of the source field to a block-edge nearest the source field as, respectively, 0, 25, 75, 125, 200, 300, 400, 500 m. Kernels of the white maize that were pollinated by the yellow variety were also yellow, thus making it easy to determine the percentage of outcrossing simply by counting the numbers of white and yellow kernels on selected ears in the white-maize blocks. The percentages of outcrossing for all three years, and also for their average, are shown in Fig.12. The quantity plotted is the percentage of the number of grains, averaged over the block, that has been fertilised by the yellow maize, as a function of distance.

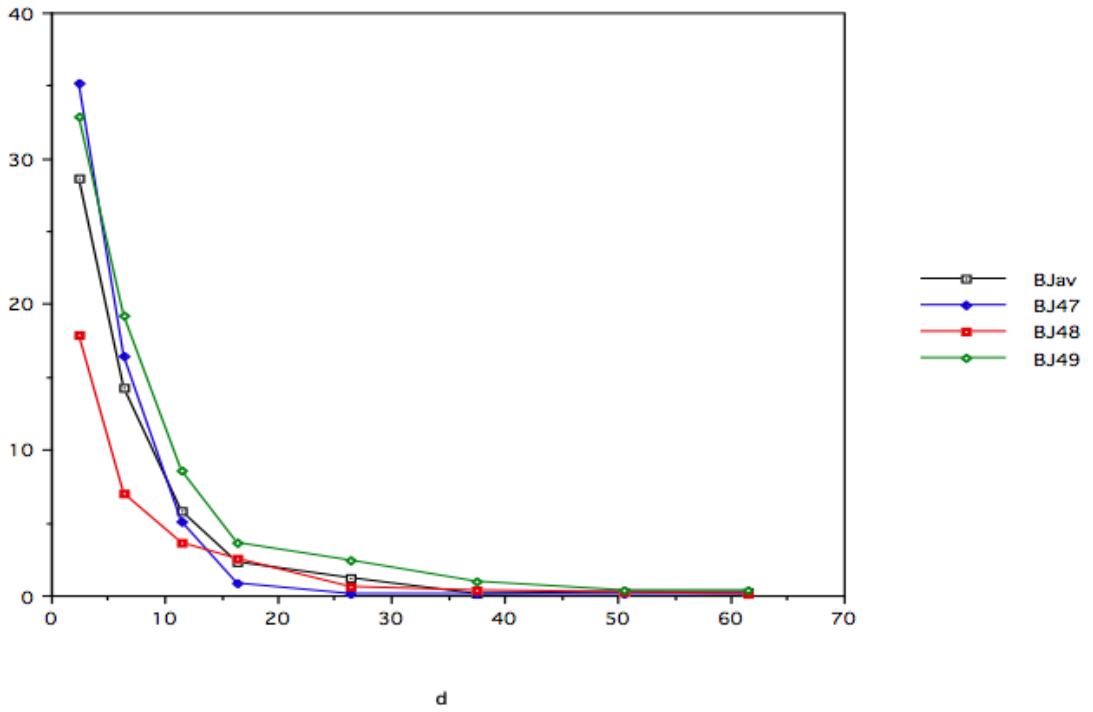

Fig. 12. Percentage of outcrossing vs. distance for data of Jones and Brooks: 1947 (blue), 1948 (red), 1949 (green), and average (black). (Distance d in numbers of CA cells; 1 cell = 8 m)

5.4 Model experiments on outcrossing compared with field observations

We now compare these observations with CA models simulating the geometry of the source field and blocks. The source field had 15 cells in the direction along the length of the lattice, and each (square) block contained 9 CA cells. Two types of pollen were tracked, one type originating in the source field and the other originating in the blocks, representing the pollen from the yellow and white maize, respectively. We assumed that the amount of deposit of pollen was proportional to the amount of outcrossing by that type of pollen. Sticking probability, P_s,was assumed to be the same for the two types of maize and, for the vegetation outside the blocks, a sticking probability half that inside the blocks and source field was assumed. Two CA parameters, P_s and v, were varied in the models:

in Exp1, $P_s = 0.1$, $v = 1.0$;
in Exp2, $P_s = 0.2$, $v = 1.0$;
in Exp3, $P_s = 0.1$, $v = 0.5$;
in Exp4, $P_s = 0.2$, $v = 0.5$.

Physical scaling of the CA models was done by, firstly, establishing the physical cell-size as $\Delta s = v\Delta t$ and then obtaining distance by multiplying the cell-size by the number of cells from the edge of the source field to a given position.

At the end of the computer run, the numbers of pollen grains of the two types in each cell had been stored, and the percentages of number of source-field ('yellow') pollen grains within each block could be calculated. The results are plotted in Figs.13-15, showing percentage of source-field pollen measured at various distances from the edge of the source field.

For each year of observations by Jones and Brooks, their results are plotted together with those of the four CA models. The right-hand panel of each Figure is logarithmic in the ordinate, to provide a better comparison amongst the curves at large distance, although, as we shall explain later, the observations and models are not expected to agree in that range. At large distances, some CA values fell to zero and therefore could not be plotted logarithmically. We may note the following results:

a) For 1947, the observed curve (black) fits rather closely to Exp3 (green curve).

b) For 1948, the observed curve (black) fits rather closely to Exp2 (yellow curve), except at the initial point.

c) For 1949, the observed curve (black) fits rather closely to Exp3 (green curve) up to and including the fourth point; but from the fifth point onwards, it fits closely to Exp1 (red curve).

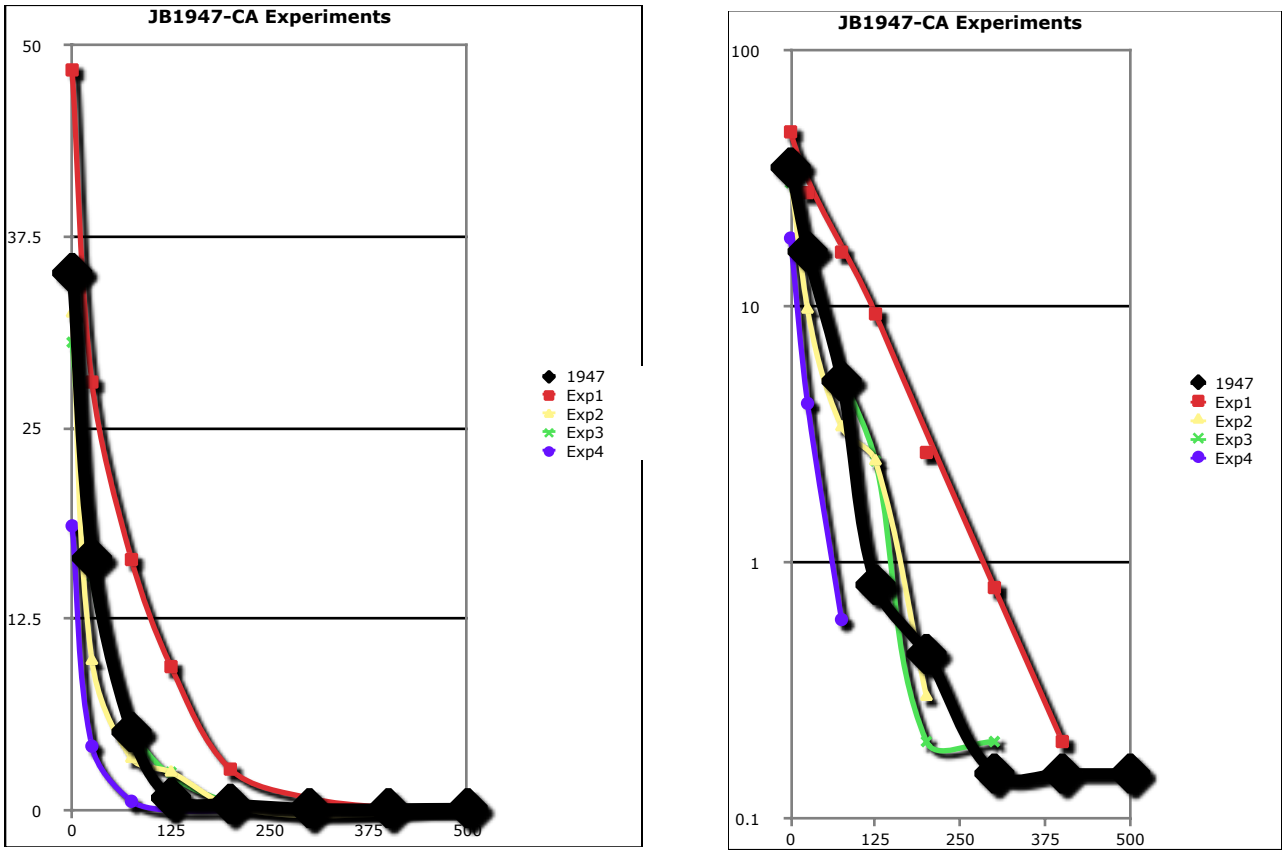

Fig. 13. Observations for 1947 by Jones and Brooks (black curves) and CA models of percentage of outcrossing with distance (expressed in metres): Exp1, red curves ($P_s = 0.1$, $w = 1.0$); Exp2, yellow curves ($P_s = 0.2$, $w = 1.0$); Exp3, green curves ($P_s = 0.1$, $w = 0.5$); Exp4, blue curves ($P_s = 0.2$, $w = 0.5$. The sharp upturn at the end of the logarithmic green curve is not the experimental result, but the result of the smooth approximation to the discrete experimental points.

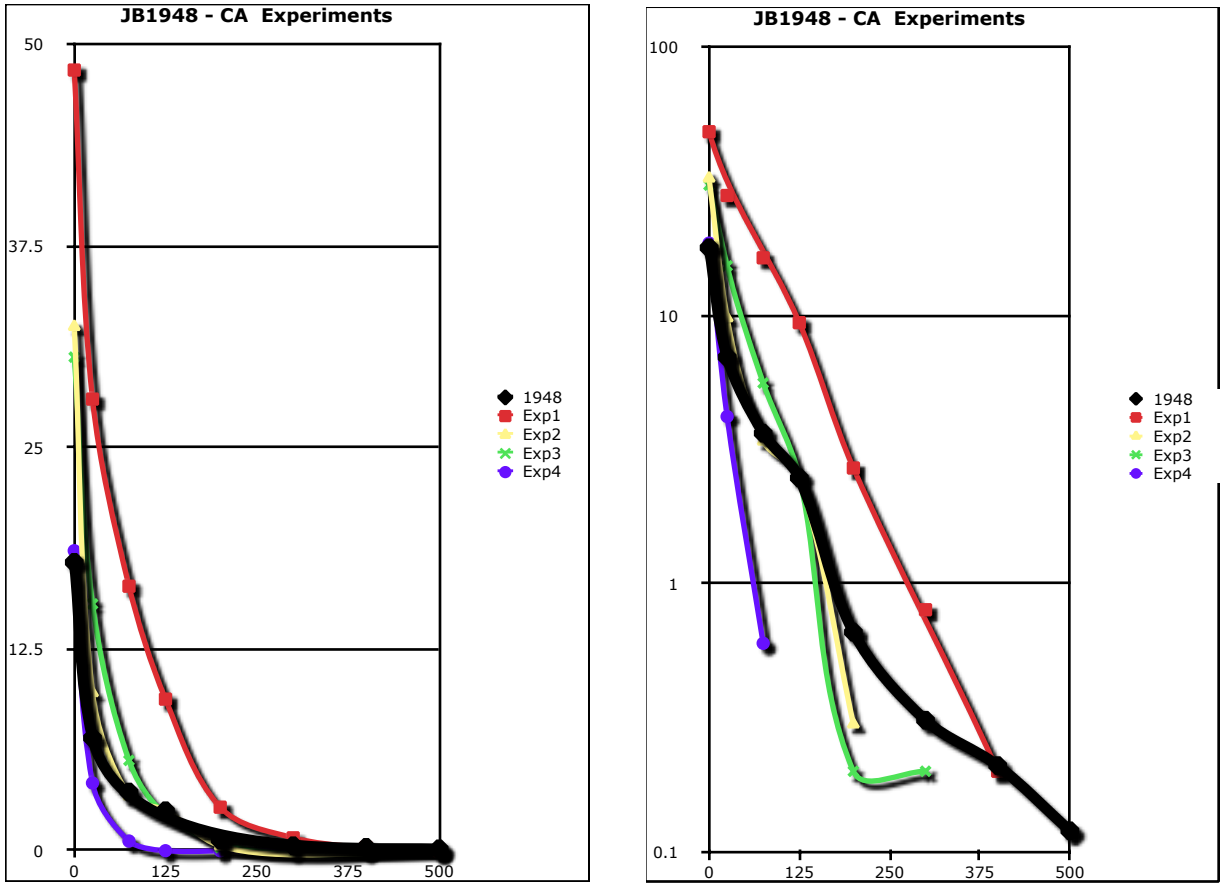

Fig. 14. Observations for 1948 by Jones and Brooks (black curves) and CA models of percentage of outcrossing with distance (expressed in metres): Exp1, red curves ($P_s = 0.1, w = 1.0$); Exp2, yellow curves ($P_s = 0.2, w = 1.0$); Exp3, green curves ($P_s = 0.1, w = 0.5$); Exp4, blue curves ($P_s = 0.2, w = 0.5$).

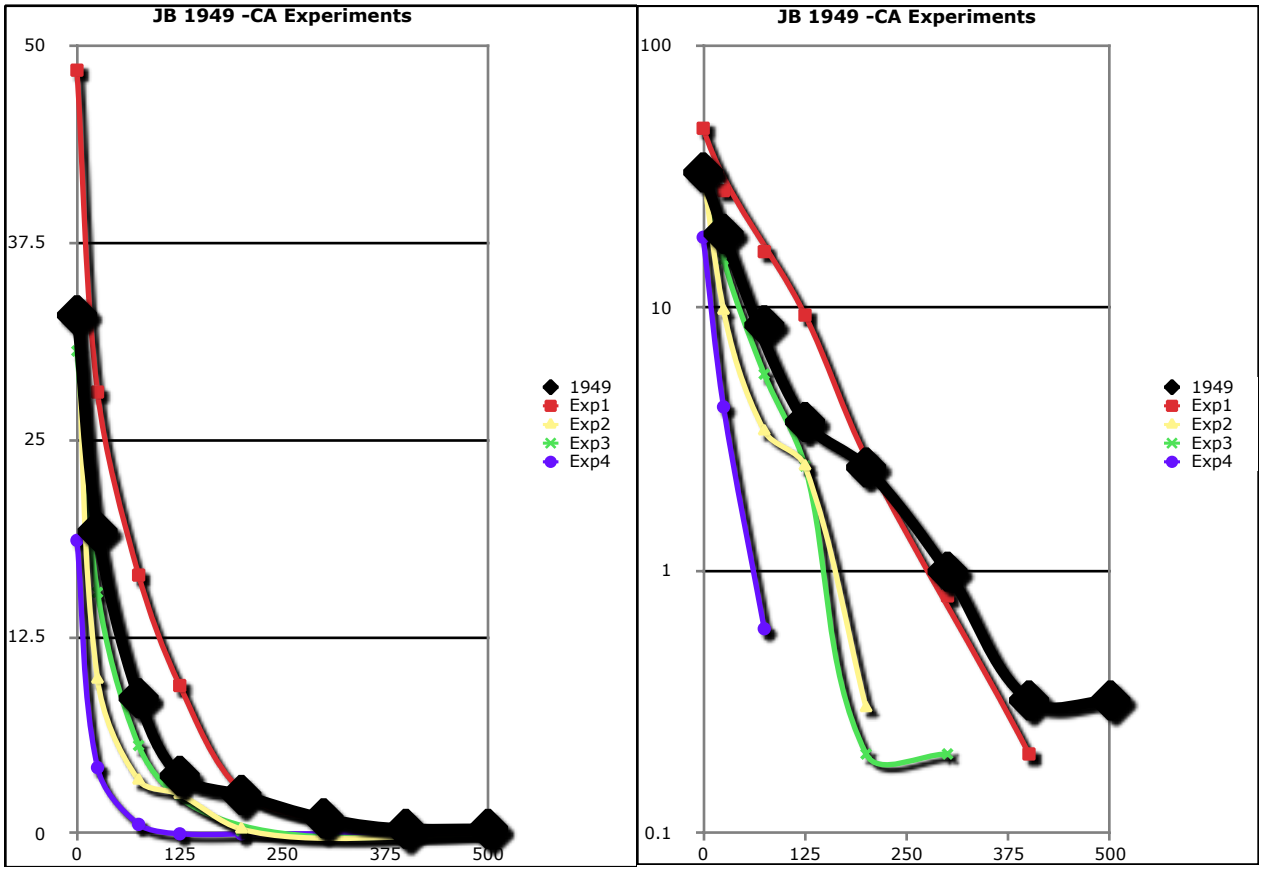

Fig. 15. Observations for 1949 by Jones and Brooks (black curves) and CA models of percentage of outcrossing with distance (expressed in metres): Exp1, red curves ($P_s = 0.1$, $w = 1.0$); Exp2, yellow curves ($P_s = 0.2$, $w = 1.0$); Exp3, green curves ($P_s = 0.1$, $w = 0.5$); Exp4, blue curves ($P_s = 0.2$, $w = 0.5$).

To understand these results, we first note that high wind-speed and low sticking probability will allow pollen to travel farthest: this is confirmed in Exp1. Conversely, low wind-speed and high sticking probability will cause pollen to be deposited over the smallest distances, as in Exp4. If

sticking probability is doubled (Exp 2 compared with Exp1), pollen travels about half as far, a result obtained also by halving the wind-speed (Exp3 compared with Exp1).

It is evident from Fig. 15 that the 1949 season experienced a shift in either wind conditions or in weather conditions (and hence sticking probability), causing the observed curve to switch from one CA curve to another. We may also note from Fig. 12 that, for 1948, the observed curve lies below the other observed curves at most distances and that it also lies below the green CA curve in Fig.14, which was the best fit for 1947 and 1949. Jones and Brooks commented: "Rainy weather and low wind velocity [in 1948] during much of the pollinating season probably contributed to the low percentage of outcrossed grain."

We may conclude from these comparisons that CA models can provide reasonable representations of pollen deposit with distance under given wind conditions. Further field observations would be needed, however, to determine appropriate values for sticking probabilities for various crops under a variety of weather conditions, as well as for critical wind-speed, v_c , and entrainment factor, f_v.

5.5 Observations of pollen deposit at large distances

An interesting feature of the data of Jones and Brooks (1950) becomes evident if the vertical scale is plotted as the logarithm of the percentage of outcrossing, which exaggerates the scale for the small percentages at large distance. This way of plotting also has the advantage of separating two transport mechanisms: at smaller distances the transport is due to the low altitude wind, which is the only mechanism we have been treating in our numerical simulations; but the tail of the distribution is likely to be the result of a second transport mechanism, namely, transport by higher-altitude wind that results in a general background of pollen, from perhaps various sources, over a large area.

In Fig. 16, where natural logarithms are used, the vertical separations between the curves therefore become more marked towards the right, until a distance of about 40 rods or 200 metres is reached. Thereafter the curves come closer together, and two of them remain at a constant level in the last interval plotted. It is likely that a very long tail persists beyond the last distance shown.

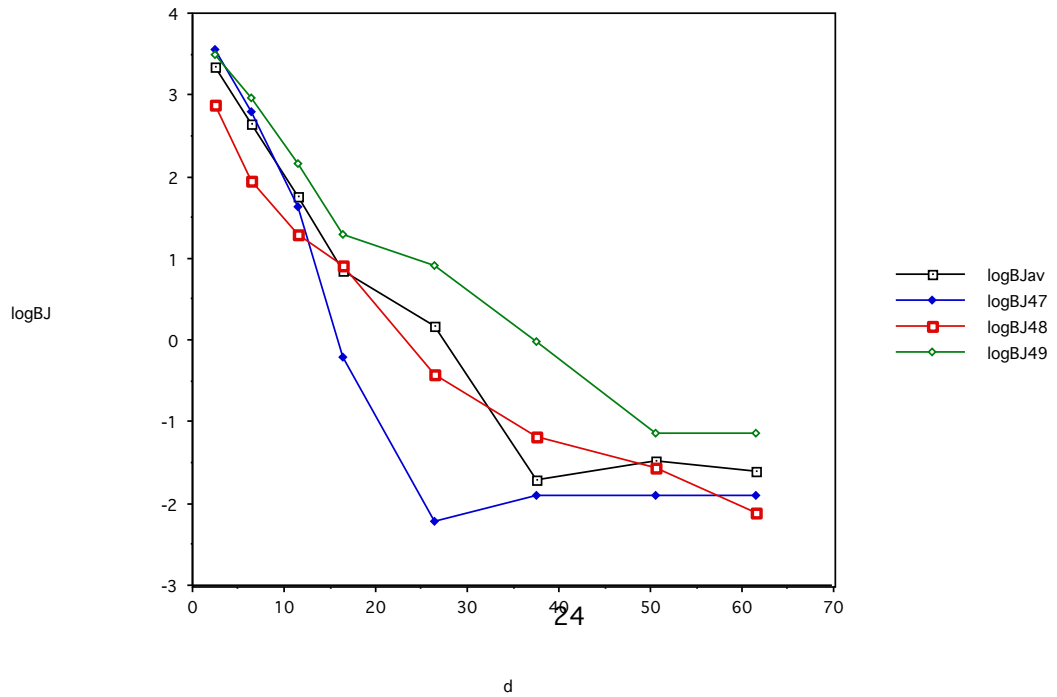

Fig. 16. Natural logarithm of percentage of outcrossing as a function of distance, from data of Jones and Brooks (1947, 1948, 1949 and average). Distance d is in CA units of length, *i.e.*, cellsize, corresponding to 8 m in the present series of experiments.

Salamov (quoted in Jones and Brooks,1950, p. 4) measured percentages of outcrossing of white maize with a yellow variety growing in the Northern Caucasus. Observations were made not only in the range of distances studied by Jones and Brooks but also beyond. In spite of the fact that Salamov's receptor maize was in the direction *opposite* to that of the prevailing winds with respect to the source field, the percentages of outcrossed maize at distances 80, 100, 120, 140 and 160 rods (400 m to 800 m) were, respectively, 0.02. 0.08, 0.79, 0.18, and 0.21 (as tabulated by Jones and Brooks, 1950, table on p. 5). The value 0.79% at 600 m is dangerously close to the value 0.9% in the European Union for permitted levels of adventitious contamination of non-GM crops by GM crops. Pollen can be carried to such large distances at higher altitudes, from where it flows downwards by various means.

Amongst other studies of long-distance pollen transport is the work on the pollen of *Betula* (birch) by Hjelmroos (1991), who measured pollen grains originating in southwestern Russia, the Baltic states and Poland that were transported to Sweden and Finland: the distances were larger than 2000 km in some cases. Yet "the pollen grains still caused considerable allergic reactions among sensitive persons." Travel times ranged from 9 to 50 hours.

In the American state of Illinois, a farmer who grew a rare blue maize for the first time received complaints from three neighbouring farmers, one of whom was 3 miles away in a cross-wind direction, that their yellow maize cobs were being noticeably contaminated with blue kernels. There was no apparent explanation except for wind transport of the pollen (Novotny, private communication; details available upon request).

6. Discussion

Using approximations to observed wind-speeds and directions and to observed pollen creation and release with time, the CA model has been able to produce results on pollen deposition that are similar to those measured in a set of published field experiments.

Numerical experiments using our CA automaton demonstrate the strong dependence of pollen-deposition patterns on wind velocity, particularly on its speed. When winds are strong, pollen is dispersed to larger distances than at times of normal conditions; in fact, these distances scale with the wind-speed. Various complex wind components such as turbulence and gusting are also important. One characteristic common to all the contour plots is the patchiness of the deposited pollen. The patchiness occurs because ever-present eddies in the air currents will move pollen about at random, requiring modelling by a probabilistic release and deposition of pollen, as is done in our CA method. The patches may take the form of isolated islands or long fingers. The detailed data of Jones and Brooks (1950, Table 3) for individual rows in the blocks during 1949 also show irregularities.

An important result of our experiments is that separation distances, intended to avoid pollination of one crop by another (as in the case of 'co-existence' between genetically modified (GM) and non-

GM crops) cannot be assigned reliably. Firstly, the region over which pollen travels is strongly dependent on the speed and direction of winds during the time that the pollen is being released. Thus, if unusually strong winds occur during the period of pollen release, the pollen will be deposited at much greater distances from the source field than under more usual conditions. In addition, separation distances are set for an average level of outcrossing over a whole field. If the individual plants of the harvested crop are sold, as for 'corn-on-the-cob', the presence of long fingers and islands of high pollen deposition shown by our numerical experiments demonstrates that it is impossible to guarantee that no produce will fall foul of the legal limit for contamination by another variety.

7. Conclusions

The CA model is a self-contained, transparent tool for simulating pollen flow. Although it would be difficult to set precise experimental values for certain parameters, notably the sticking probability, CA modelling can nevertheless be used to determine the general characteristics of the patterns of deposited and air-borne pollen over an area. Inputs to the modelling, including topography, barriers, characteristics of the wind, dispersal of pollen by insects, details of pollen production and release, effects of moisture and other relevant factors can, at the discretion of the programmer, be either ignored or incorporated to any degree of simplicity or complexity.

None of the simulations was continued long enough to allow all the air-borne pollen to settle, but the air-borne pollen will eventually have to come to ground. The role of high-altitude winds has not been explored in these numerical experiments. Both intuition and a dimensional argument, as well as observations, make it obvious that such winds disperse pollen over much larger distances than the ground-wind component. Atmospheric effects such as convection, convective storms and frontal storms can transport pollen for hundreds of kilometres, in some cases in times short enough that the pollen might remain viable (Emberlin, Adams-Groom and Tidmarsh, 1999).

Acknowledgments

We are grateful to the UK Meteorological Office for supplying data on wind velocities and for clarifying various details, and to the National Pollen Research Unit at University College Worcester for providing us with copies of some of the reference papers. We thank the Institute of Astronomy, Cambridge, for use of the premises during most of this work.

References

Emberlin, J., Adams-Groom, B., Tidmarsh, J., 1999. A Report on the Dispersal of Maize Pollen. Commissioned by The Soil Association.

Hjelmroos, M., 1991. Evidence of long-distance transport of *betula* pollen. Grana 30, 215-228.

Jones, M. D., Brooks, J.S., 1950. Effectiveness of Distance and Border Rows in Preventing Outcrossing in Corn. Oklahoma Agricultural Experimental Station Technical Bulletin No 38.

Jones, M.D., Newell, L.C., 1946. Pollination Cycles and Pollen Dispersal in Relation to Grass Improvement. University of Nebraska College of Agriculture, Agricultural Experiment Station, Research Bulletin No 148.

Novotny, E., Perdang, J., 2002. Chardon LL Hearing Report III (for Scientists for Global Responsibility), http://www.sgr.org.uk/resources/chardon-report-iii-model-pollen-transport-wind).

Novotny, E., Perdang, J., Paper I, Simulation of Pollen Transport by Wind: The Cellular Automaton Model, http://www.sgr.org.uk/sites/sgr.org.uk/files/PollenTransport-Paper%20I-final-SGR.pdf

Salamov, A.B., 1940. Sel. i. Sem, 3 (Russian trans. by Michel Afanasiev in 1949), as reported in Jones and Brooks, 1950, p. 4.